RFI as Experienced During Preparations for the SMOS Mission

Niels Skou[1], Sidharth Misra[2], Sten S. Søbjærg[1], Jan E. Balling[1], and Steen S. Kristensen[1]

[1]National Space Institute, B 348. Technical University of Denmark.
DK 2800 Lyngby, Denmark.
Phone: (45) 45 25 38 00, Fax: (45) 45 93 16 34
e-mail: ns@space.dtu.dk, sss@space.dtu.dk, jeb@space.dtu.dk, ssk@space.dtu.dk

[2]Space Physics Research Laboratory, University of Michigan
2455 Hayward St., Ann Arbor, MI 48109-2143, USA.
Phone: (1) 734 647 3450, Fax: (1) 734 763 5567
e-mail: samisra@umich.edu

Abstract

RFI (radio frequency interference) is a possible threat to coming spaceborne L-band radiometer missions. Ground based and airborne campaigns report some level of interference that must be detected and possibly mitigated. Methods to do so are discussed and demonstrated.

1. Introduction

Radiometer signals received in the L and C band are particularly susceptible to man-made radio frequency interference [1, 2]. RFI detection and possibly mitigation has become an important issue, as both ESA and NASA plan to launch satellite missions, SMOS and Aquarius respectively, measuring sea surface salinity (SSS) and soil moisture in the L-band.

2. About Kurtosis, Detection of RFI, and Mitigation

The microwave radiometer generally detects natural thermal emissions as well as thermal noise of the hardware. These signals are random processes and hence the amplitude of the signal has a Gaussian distribution. The kurtosis algorithm for RFI detection discussed in [3] takes advantage of the fact that almost all man-made sources would have a non-Gaussian distribution. RFI is detected by measuring the amount of deviation of the kurtosis parameter from normality. The kurtosis algorithm measures the higher order central moments of the incoming radiometer signal to obtain the kurtosis. The 2^{nd} central moment (variance) obtained over a particular integration period is equivalent to the system noise temperature measured by the radiometer – i.e. it is the output of a traditional radiometer, and what we know as the measured brightness temperature (after proper calibration). The ratio of the 4^{th} central moment to the squared 2^{nd} central moment gives the kurtosis ratio, k, and for natural thermal emissions it should ideally be equal to 3. If the signal is corrupted by man-made RFI, the distribution should deviate from normality and thus k should deviate from 3. This property can be used to flag RFI contaminated signals. Since the algorithm is insensitive to change in the 2^{nd} moment, natural variations in the brightness temperature will not be falsely flagged as RFI.

A traditional radiometer measures as already mentioned the 2^{nd} order central moment. This can be done in a variety of ways:

1. the signal is detected by a square law detector, pre-integrated to reduce bandwidth, sampled and A-to-D converted, integrated digitally to match the dwell time per footprint (could be 1 sec in airborne and spaceborne instruments), and finally stored or down-linked.
2. as (1), but the data is not integrated before storage or down-link. The price to pay is increased requirements to storage capacity or down-link bandwidth – the gain is increased flexibility and new options concerning signal processing.
3. the signal is NOT detected by an analog detector, but directly sampled obeying Nyquist. This results in the ultimate in flexibility and signal processing possibilities. The drawback is of course high sampling rates and fast data processing. Even at L-band the signal bandwidth is typically 25 MHz meaning that the sampling rate has to be beyond 50 MHz

From an RFI detection and mitigation point of view (1) is not very good. First of all no special data processing can be carried out to detect RFI. One can only observe each footprint and look for unusually large TB values. As RFI is normally of a pulsed nature, even large signals may be integrated to a few Kelvins over the long integration time – resulting in false signals that are very difficult to detect yet still very harmful. Moreover, if RFI is detected, a full footprint will have to be discarded – even if the original RFI signal was of very short duration.

Instruments operating according to (2) are in a somewhat better position concerning both RFI detection and mitigation. Since we have less integration, large radar type spikes are much easier to detect, and we only have to discard maybe a few samples within a footprint. Let us consider an example where data is sampled and transmitted to ground with 10 msec rate for final integration to 1 sec to match the dwell time per footprint. Lets further assume that in one of the 10 msec samples we find one radar spike corresponding to a 200 K increase of the TB of that sample. After final integration to 1 sec this spike will give a 2 K contribution to the footprint TB. This is very difficult to detect by traditional means, yet the contribution is detrimental! In contrast, the signal is very easy to detect when inspecting the individual samples. A key parameter in such systems is of course the choice of pre-integration, hence data rate to be stored or down-linked. The higher the data rate, the better from an RFI perspective.

Instruments operating according to (3) possess a wealth of possibilities. Due to the very high data rate / very short integration, even radar pulses (could typically be of μsec. duration) are resolved and quite easily detected. Discarding such contaminated samples in general means that only a very small percentage of data is lost. Even more important, signal processing can be applied to the data stream, as for example the calculation of kurtosis as described previously. This enables a very safe flagging of RFI with low false alarm ratio. The airborne EMIRAD-2 digital radiometer system, as used in the CoSMOS campaigns in preparation for the SMOS satellite, operates according to this principle [4, 5]. The data from the A-to-D converters is fed into a fast FPGA where the TB data is integrated to 8 msec and output to storage ("slow data" for normal users) and also only integrated to 1.8 μsec before output to storage ("fast data" for special investigations). Moreover, kurtosis is calculated for the same two time intervals (8 msec and 1.8 μsec) and output to storage.

3. RFI as Experienced During the CoSMOS campaigns

The EMIRAD-2 system has been used in airborne campaigns over ocean (the North Sea west of Norway) over land (Australia), and in coastal regions close to Helsinki. Figure 1 shows typical data examples.

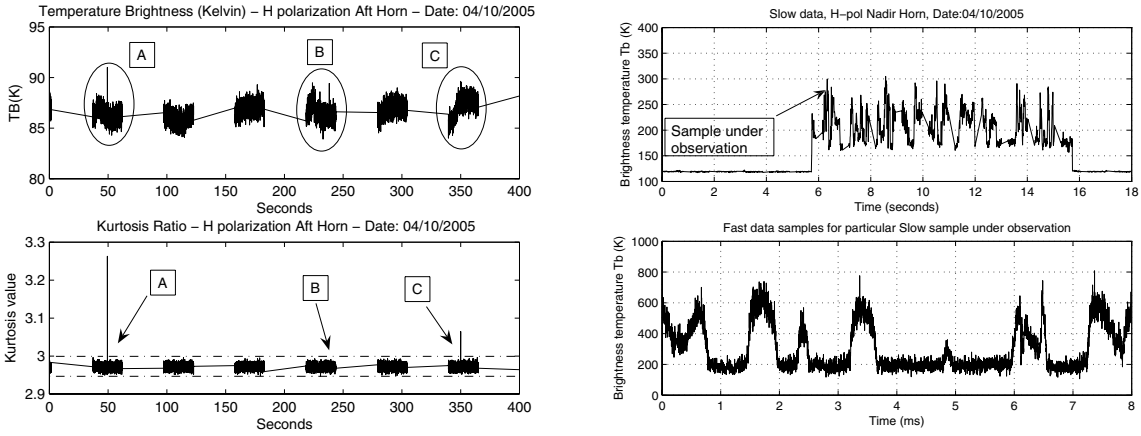

Figure 1: to the left normal brightness data and associated kurtosis, to the right normal 8 msec slow data and one sample resolved to 1.8 μsec (fast data)

To the left is shown 400 seconds of slow data measured by the aft-horn, with the top plot indicating TB (in Kelvin) and the bottom plot indicating the kurtosis. The dashed lines in the bottom plot indicate the kurtosis thresholds within which data is considered to be RFI free. The thresholds are based on the noise-margin of the kurtosis statistics. The kurtosis mean is slightly less than 3 due to factors like digitization, number of samples, a.o. Cases A and C shown in the plots are flagged as RFI. Comparing them it is noticed from the top plot that there is a clear spike in the brightness data for the first case (A), whereas there is negligible difference in the value of the

second case (C) compared to its surroundings. This demonstrates the ability of the kurtosis algorithm to detect man-made interference near the noise-margin of the radiometer data. Case B is a counter example, where the TB plot clearly indicates a spike, and this might cause the data sample to be falsely flagged as RFI if some kind of threshold algorithm were used. On the other hand the bottom plot indicates the kurtosis completely within the set noise-margins, thus demonstrating that the sample is a part of a natural thermal emission. Each slow data sample integrated over a period of 8msec, has approximately 4500 corresponding fast data samples as shown to the right in Figure 1. If any slow data sample is flagged as RFI by kurtosis, by observing the associated fast data samples it is possible to measure the exact amount of RFI contribution to the measured temperature value: the integrated value is calculated before and after discarding all the obvious RFI spikes. It is also seen that such fast sampling offers an alternative to kurtosis flagging of RFI as the RFI spikes generally are very visible.

The 8 msec data from all CoSMOS campaigns has been processed, and properly flagged using the kurtosis method. Following that, the percentage of data that has been flagged is calculated, see Table 1.

RFI percentage for CoSMOS-OS, when over Land and Sea

	Aft Horn				Nadir Horn			
	Horizontal Pol		Vertical Pol		Horizontal Pol		Vertical Pol	
Date	Land	Sea	Land	Sea	Land	Sea	Land	Sea
06-apr	5,827	0,436	6,587	0,533	9,327	0,314	4,797	0,487
09-apr	0,736	0,059	5,214	0,366	7,131	0,062	8,828	0,435
10-apr	3,592	0,026	5,060	0,356	6,397	0,046	1,670	0,429
12-apr	0,551	0,035	1,532	0,307	1,328	0,043	7,874	0,356
13-apr	1,415	0,574	3,113	1,023	5,854	0,868	8,363	1,163
15-apr	1,144	0,054	2,357	0,616	2,047	0,059	5,428	0,721
16-apr	13,635	1,967	16,424	2,436	19,523	3,373	15,791	1,519
18-apr	1,914	0,131	1,358	0,456	0,307	0,055	4,011	0,556
19-apr	3,824	0,701	6,674	1,450	6,847	2,388	5,539	0,899
22-apr	2,936	35,991	15,291	41,569	23,360	43,947	2,753	18,004
25-apr	0,620	0,054	2,227	0,270	4,382	0,062	1,954	0,293
29-apr	26,043	31,198	36,157	35,400	41,698	53,340	19,067	18,711
30-apr	2,365	0,985	3,572	0,280	1,223	0,441	3,054	0,599

RFI percentage for CoSMOS-Aus

	Aft Horn			Nadir Horn		
Date	Horizontal Pol	Vertical Pol		Horizontal Pol	Vertical Pol	
15-nov	2,995	0,833		14,96		2,5832
27-nov	2,2621	0,5486		17,359		2,6892
29-nov	2,9446	0,7822		15,996		1,2194
03-dec	5,4427	5,698		29,987		5,3384
06-dec	4,0304	2,0951		21,769		4,973

Table 1: RFI percentages, Norway and Australia

Apart from a couple of special days with excessive RFI, the following observations can be made: In Norway the percentages over sea are markedly below those over land. Actually not much land was covered during these missions, and the land that was covered is close to the airport, so this is not so strange, but only adds to the general suspicion that airports are often strong emitters of RFI. It is seen that the percentages over sea are very modest, and a recommendation could be: discard all flagged data before entering into analysis, and do not even worry about the fact, that then some data, where the RFI is really not harmful, is lost. The loss of data is anyway totally insignificant. Concerning the Australian data set the percentages are somewhat higher, but still manageable in most cases, see also next paragraph. The percentages from the Finland mission are much in line with the Norway numbers.

The flagging procedure as discussed until now can be regarded as overly conservative: the method is very sensitive, and data may well be flagged even though the RFI contribution to the brightness temperature is below a fully acceptable level. Using the fast data as described before, it was found that more than 50% of the flags correspond to RFI contributing less than 1 K when considering data integrated to 1 sec. And actually a major part is even below 0.1 K. Also, it is important to check for example the Australian data to see where actually the flags are geographically. By plotting the flags versus latitude and longitude, it turns out that a major part clusters around the airport and urban areas, with very few flags in the rural area where the soil moisture campaign was carried out.

4. Use of 3rd and 4th Stokes Parameters

The EMIRAD-2 data sets have shown that the 3rd and 4th Stokes parameters of RFI-flagged data samples often exhibit substantial deviation from what is seen when observing RFI-free data samples. This may form a useful basis for the detection and mitigation of RFI in a data set where use of the kurtosis algorithm is not possible. In order to evaluate the possibilities of detecting genuine RFI as well as the risks of falsely flagging clean data samples

as RFI-contaminated ones, a data set from the CoSMOS-OS campaign has been investigated. The data set under observation is the same as the one discussed in section 2, however, investigations have been limited to data acquired over the open sea during transit where aircraft attitude variations are negligible. An expected brightness temperature in the vertical channel of the radiometer has been calculated by integrating the data through a 20-sample-wide moving window, corresponding to an uncertainty of 0.2 K. Then, the relationship between deviations from this expected brightness temperature and the behavior of the 3rd and 4th Stokes parameters has been investigated. An example, showing how TB deviations relate to changes in the 3rd and 4th Stokes parameters can be seen in Figure 2.

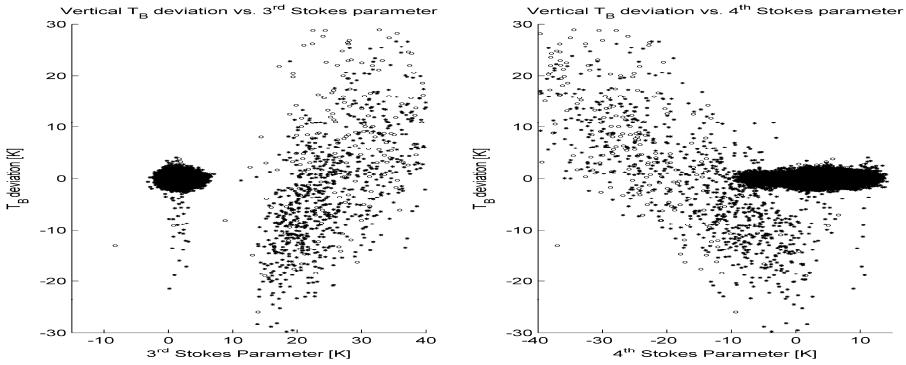

Figure 2: to the left TB deviation (vertical) vs. the value of the 3rd Stokes parameter, to the right TB deviation (vertical) vs. the value of the 4th Stokes parameter. Hollow circles denote data samples flagged as RFI contaminated by the kurtosis algorithm.

More than 98% of the examined data samples exhibit TB deviations within an interval of ±5 K and deviations of the 3rd and 4th Stokes parameters within ±5 K and ±10 K, respectively. A part of these samples (0.36%), however, have been flagged by the kurtosis algorithm as being contaminated with RFI, whereas RFI-contaminated data account for about 8% of the data samples situated outside these intervals. Hence, large variations in the value of the 3rd and 4th Stokes parameters cannot be considered reliable RFI markers in their own right.

As a simple illustration, RFI mitigation has been carried out by discarding all data samples with 3rd as well as 4th Stokes parameters outside the above-mentioned limits. This resulted in 1.39% of the total samples being discarded, 28% of the flagged samples being caught and 1.26% of the clean samples erroneously being discarded. Requiring the samples to fall within both limits raised the amount of caught samples to 35% but on the other hand also increased the amount of erroneously discarded samples to 9%.

6. Conclusions

In this paper, three different approaches to acquiring radiometric data and their impact on subsequent RFI detection and mitigation have been discussed. Also, two different RFI detection schemes have been demonstrated: The first one, based on the kurtosis algorithm, requires that data is acquired by means of a radiometer which makes the 4th central moment available, whereas the second scheme relies on observation of the 3rd and 4th Stokes parameters. It has been demonstrated that this RFI detection scheme is inferior to the one based on the kurtosis algorithm; less than a third of the data samples flagged by the kurtosis algorithm is found by inspection of the 3rd and 4th Stokes parameters.

7. References

1. E. G. Njoku, P. Ashcroft, T. K. Chan, and L. Li, “Global survey and statistics of radio-frequency interference in AMSR-E land observations,” *IEEE Trans. Geoscience and Remote Sensing*, vol. 43, May 2005, pp. 938-947.
2. D. M. Le Vine and M. Haken “RFI at L-band in synthetic aperture radiometers,” in *Proc. IGARSS’03*, vol. 3, Tolouse, France, July 2003, pp. 1742-1744
3. C. S. Ruf, S. M. Gross, and S. Misra, “RFI Detection and Mitigation for Microwave Radiometry with an Agile Digital Detector,” *IEEE Trans. Geoscience and Remote Sensing*, vol. 44, March 2006, pp. 694-706.
4. N. Skou, S. S. Søbjærg, J. Balling, and S. S. Kristensen, "A Second Generation L-band Digital Radiometer for Sea Salinity Campaigns," *Proc. IGARSS'06*, Denver, USA, July 2006, 4 p.
5. S. Misra, S. S. Kristensen, S. S. Søbjærg, N. Skou, “CoSMOS, “Performance of Kurtosis Algorithm for Radio Frequency Interference Detection and Mitigation”, *Proc. IGARSS’07*, Barcelona, Spain, July 2007, 4 p.